İSTANBUL UNIVERSITY CERRAHPAŞA

ORIGINAL ARTICLE
Electrica 2025; 25: 1-14

Assessing Ampacity Performance Through Dynamic Line Rating: A Comparison of IEEE Std 738 and CIGRÉ TB 601

Ziauddin Zia, Celal Fadil Kumru

Süleyman Demirel University, Faculty of Engineering and Natural Sciences, Electrical-Electronics Engineering Department, Isparta, Türkiye

Cite this article as: Z. Zia and C. F. Kumru, "Assessing ampacity performance through dynamic line rating: A comparison of IEEE std 738 and CIGRÉ TB 601," *Electrica*, 2025, 25, 0109, doi: 10.5152/electrica.2025.25109.

WHAT IS ALREADY KNOWN ON THIS TOPIC?

- *DLR methods are used to enhance transmission line capacity by considering real-time meteorological and loading conditions.*
- *IEEE and CIGRÉ have developed widely adopted thermal models for estimating conductor ampacity.*
- *Most studies focus on theoretical evaluations or short-term field tests, and standard comparisons are often limited.*

ABSTRACT

Overhead transmission lines (TLs) are typically rated using static methods that assume conservative environmental conditions, such as high ambient temperatures and low wind speeds. These conservative ratings often result in underutilization of the line's full ampacity, as extreme conditions occur only intermittently. Dynamic line rating (DLR) addresses this issue by utilizing real-time weather and grid load data to dynamically calculate the available ampacity, considering favorable environmental conditions. The DLR continuously updates ampacity calculations, allowing operators to access unused capacity when conditions are more favorable. This approach improves transmission efficiency and enhances grid reliability, ensuring a more adaptive and resilient power system. By integrating real-time weather data, DLR provides a more accurate representation of a TL's actual capacity than static ratings. Both IEEE and CIGRÉ standards employ the heat balance equation to calculate ampacity, accounting for heat absorption and dissipation. This paper compares the methodologies outlined in IEEE Std 738 and CIGRÉ TB 601, focusing on their approaches to calculating conductor temperature and ampacity. The study examines the impact of different modeling approaches on ampacity calculations and the performance of TLs. The analysis shows significant differences between the two methods. In summer, the IEEE method increases ampacity by 47.2% compared to static line rating (SLR), while the CIGRÉ method increases it by 46.5%. In winter, the IEEE method shows a 36.9% increase, and CIGRÉ shows a 38.6% increase. These results demonstrate the potential of DLR to optimize transmission capacity and improve grid performance by adapting to real-time environmental conditions. Seasonal variations further highlight how factors like temperature and wind speed impact ampacity, reinforcing the value of DLR systems for maximizing TL efficiency year-round.

***Index Terms*—**Ampacity, dynamic line rating, grid reliability, real-time weather data, seasonal variation, transmission lines

I. INTRODUCTION

The capacity of overhead TLs to carry electrical current is limited by thermal constraints, primarily governed by the conductor's physical properties [1–3]. Traditionally, transmission capacity has been determined using static or seasonally adjusted values based on conservative assumptions such as persistently low wind speeds and high ambient temperatures throughout the year or season [4, 5]. However, since such extreme conditions occur only briefly, this approach often results in underutilization of existing infrastructure. In practice, conductor cooling driven by real-time weather conditions frequently allows for additional ampacity that remains untapped [6]. The DLR is a technology that determines the real-time capacity of TLs by calculating the balance between thermal energy absorbed and dissipated in the conductor, as illustrated in Fig. 1. By incorporating real-time monitoring of both electrical and environmental parameters, DLR significantly improves line utilization, especially for critical overhead TLs. Recent research has demonstrated that DLR can be integrated with flexible network topology strategies to actively manage congestion in urban power grids. By dynamically adjusting network configurations alongside real-time conductor ratings, transmission capacity can be maximized without extensive infrastructure upgrades. This approach also supports the prioritization of critical loads and allows for more efficient utilization of renewable generation. These results indicate that combining DLR

Corresponding author:
Celal Fadil Kumru

E-mail:
celalkumru@sdu.edu.tr

Received: April 25, 2025
Revision Requested: July 20, 2025
Last Revision Received: August 29, 2025
Accepted: September 13, 2025
Publication Date: November 25, 2025

DOI: 10.5152/electrica.2025.25109

WHAT THIS STUDY ADDS ON THIS TOPIC?

- *This study presents a detailed hour-by-hour comparison of IEEE and CIGRÉ standards for a full summer day, including conductor surface temperature and ampacity profiles.*
- *Realistic weather data such as wind speed, wind direction, ambient temperature, and solar radiation are incorporated to evaluate thermal behavior under both standards.*
- *The study reveals significant temperature and ampacity differences between the two standards, particularly under varying solar radiation, providing valuable insight for more accurate DLR-based line management.*

with topology optimization can provide both operational and economic benefits for modern smart grids [7].

The ampacity of a TL is defined by the maximum allowable conductor temperature under specific environmental conditions. Standard DLR models have been developed by leading organizations such as the International Council on Large Electric Systems (CIGRÉ TB 601) [8] and the Institute of Electrical and Electronics Engineers (IEEE 738) [9, 10].

The DLR has been gaining significant attention from governmental agencies, professional communities, and electric utilities. The U.S. Department of Energy has identified DLR as one of the eight key smart grid transmission and distribution infrastructure metrics [1], [4]. In parallel, both IEEE and CIGRÉ have established dedicated working groups to standardize methodologies for calculating overhead line temperatures under varying weather conditions [8, 10]. Specifically, IEEE has developed the IEEE Std 738 for DLR applications, while CIGRÉ has introduced several guidelines and computational models to support accurate DLR assessments [8, 11]. Several studies highlight the importance of DLR in integrating variable renewable resources such as wind power. For example, applying real-time thermal ratings improves the reliability of wind-integrated networks by enabling higher line utilization without overloading conductors. When coupled with energy storage or electric vehicle infrastructure, DLR provides a mechanism to balance generation variability and enhance grid flexibility. Additionally, the use of DLR allows system operators to respond to sudden changes in renewable output, reducing curtailment and improving overall system efficiency [12–14]. Furthermore, research communities have been actively engaged in advancing DLR technology and addressing regulatory challenges to enable more effective utilization of existing TL capacity. Recent studies have investigated various applications of DLR in power grids. In [15], the use of DLR for day-ahead planning was proposed, while another study developed a method to improve operational tripping of TLs [16]. In a different context, DLR was suggested as a solution for managing distribution congestion [17], and researchers have also explored its integration into unit commitment processes [18]. Moreover, several studies have addressed the regulatory frameworks required for the effective implementation of DLR systems [19]. Additional investigations have demonstrated that DLR can optimize distributed generation and storage allocation across networks. By combining metaheuristic algorithms with DLR, operators can ensure N-1 reliability and reduce operational costs while meeting demand and minimizing losses. This integration enables more precise scheduling of generation units and helps maintain system stability even under fluctuating load and generation conditions. These findings support the extension of DLR applications beyond real-time line rating into broader operational optimization frameworks [14, 20]. Despite these advancements, significant challenges remain in quantifying the real-world benefits of DLR. Demonstrating its effectiveness and encouraging broader adoption by electric utilities require pilot studies that incorporate actual grid operational data and localized weather conditions. Several countries have successfully implemented DLR using various methodologies to optimize transmission capacity. In 2014, Belgium's transmission system operator (TSO), Elia, applied DLR-based on the CIGRÉ methodology to increase import capacity following the shutdown of nuclear plants. This approach led to thermal rating improvements of over 200%, although actual gains were limited to 130% due to asset constraints [21, 22]. Similarly, Bulgaria and Slovenia implemented DLR to enhance system reliability and address icing issues in cross-border exchanges [21, 23]. In France, the TSO RTE began experimenting with DLR in 2009 through initiatives such as the "Ampacité" project, which focused on optimizing wind farm integration [24]. Italy's TSO, Terna, deployed (DLR) on four (TLs) to increase capacity and support wind energy integration [25]. In 2014, the U.S. utility Oncor Electric Delivery implemented DLR as well, achieving a 6%–14% increase in capacity across eight (TLs) [26, 27]. Uruguay adopted DLR in 2018 under the IEEE framework, successfully reducing wind power curtailment and enhancing renewable energy utilization [28]. Around the same time, Vietnam's smart grid roadmap recognized DLR under IEEE as a key solution for improving operational efficiency and managing the country's rapid load growth [28]. Moreover, understanding the impact of real-time thermal variability is critical for long-term reliability planning. Studies show that incorporating dynamic ratings into reliability assessments allows for better estimation of risk and asset lifetimes. Predictive models using meteorological forecasts and AI techniques can enhance the accuracy of DLR and support operational decision-making. This predictive capability is particularly valuable for managing high renewable penetration, reducing the risk of line overloads, and improving system resilience [29–33]. Furthermore, integrating DLR into cyber-physical power system frameworks has been shown to improve operational reliability and resilience. By modeling cyber threats and implementing data-driven mitigation strategies, operators can safeguard the accuracy of real-time ratings and ensure

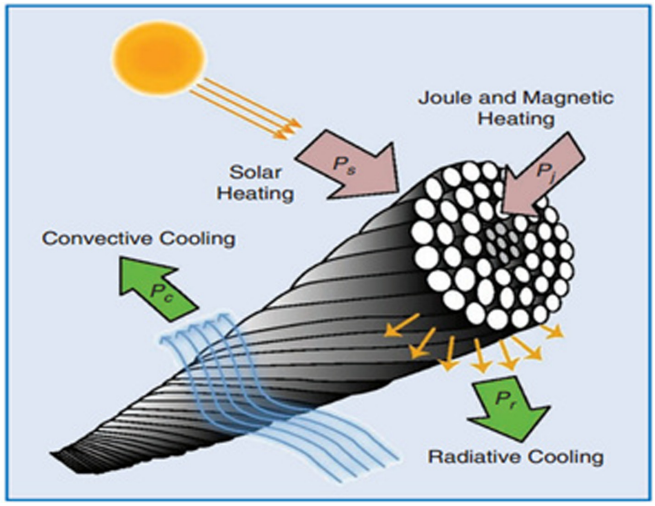

Fig. 1. A representation of the thermal equilibrium in TL conductor [5].

secure system operations. This integration highlights the broader relevance of DLR not only for operational efficiency but also for modern smart grid cybersecurity [33, 34].

Building on these global implementations, a pilot assessment of DLR for TL segments is presented in this study. An indirect method based on both IEEE and CIGRÉ methodologies is used to evaluate the potential benefits of DLR in enhancing line ampacity utilization. Actual operational data, including line loading and key meteorological parameters (wind speed, wind direction, ambient temperature, and solar irradiance), are incorporated to compare the performance of these two standards under varying weather conditions. Ultimately, the advantages of DLR are assessed by examining its impact on TL asset utilization and comparing it with static ratings based on real operational data and local weather conditions. The findings provide valuable insights for electric utilities, demonstrating the potential of DLR to optimize TL capacity.

II. METHODOLOGY

The calculation of TL ampacity (I_{max}) is presented in Table I for both IEEE and CIGRÉ methods. These methods are based on the heat balance equation, which ensures that thermal equilibrium is reached when the total heat absorbed equals the total heat dissipated [15]. According to the steady-state thermal equilibrium equation, ampacity of a TL can be calculated using (2) and (4) for IEEE and CIGRÉ, respectively.

Both standards agree on neglecting magnetic heating (P_M), evaporative cooling (P_w), and corona heating (P_i). Although corona heating can become significant under conditions of high wind speed and humidity, convective cooling remains the dominant mechanism, making the effect of corona heating negligible. Similarly, while evaporative heat loss can substantially influence conductor temperature, it is typically excluded from thermal rating calculations due to the rarity of the entire line being wet and the difficulty in accurately quantifying its impact. Joule heating (q_j and P_J) is generated by the electrical current flowing through the conductor, resulting in resistive losses that produce heat. Solar heating (q_s and P_S) refers to the heat absorbed by the conductor due to solar radiation. On the cooling side, convective cooling (q_c and P_c) involves the dissipation of heat through air movement around the conductor, while radiative cooling (q_r and P_r) refers to the emission of infrared radiation from the conductor's surface. These mechanisms are described in the IEEE 738 and CIGRÉ TB 601 standards, respectively.

The ampacity of TLs is determined by balancing these heating and cooling mechanisms, with the conductor resistance expressed as $R(T_c)$, where T_c represents the conductor temperature. The transient equilibrium, as shown in Table II for both standards, is employed to characterize the stable operating condition of conductors [35].

The product of the mass of ACSR per unit length and its specific heat capacity is represented by $m{\cdot}C_p$. The transient temperature response of the conductor plays a critical role in determining how quickly the conductor reaches a new thermal equilibrium following a sudden change in electrical loading. This behavior is crucial for accurately estimating the DLR of TLs.

This study is conducted under the specific conditions presented herein, including selected transmission line (TL) segments, particular conductor types, and local climatic parameters. Therefore, the results may not fully represent other geographical regions or alternative conductor configurations. While the findings provide valuable insights into the performance of dynamic line rating (DLR) under these specified conditions, further research is necessary to assess the applicability of these methods across diverse systems and operational scenarios.

A. Joule Heating and Solar Heat Gain

The definitions of Joule heating per unit length differ between the IEEE 738 and CIGRÉ models, with each using distinct equations to describe the phenomenon, as shown in Table III.

TABLE I. DLR HEAT BALANCE AND AMPACITY EQUATIONS AS PER IEEE 738 AND CIGRE 601

Standard	Equation	
IEEE 738	$\underbrace{q_j+q_s}_{\text{Heat gain}}=\underbrace{q_c+q_r}_{\text{Heat loss}}$	(1)
	$I_{max}=\sqrt{\frac{q_r+q_c-q_s}{R(T_c)}}$	(2)
CIGRE TB 601	$\underbrace{P_J+P_S+P_M+P_i}_{\text{Heat gain}}=\underbrace{P_c+P_r+P_w}_{\text{Heat loss}}$	(3)
	$I_{max}=\sqrt{\frac{P_r+P_c-P_s}{R_{AC}(T_c)}}$	(4)

TABLE II. DLR TRANSIENT EQUILIBRIUM AS PER IEEE 738 AND CIGRE 601

Standard	Equation	
IEEE 738	$m\cdot C_p\frac{dT_{avg}}{dt}=q_j+q_s-q_c-q_r$	(5)
CIGRE TB 601	$m\cdot C_p\frac{dT}{dt}=P_J+P_s-P_c-P_r$	(6)

TABLE III. JOULE HEATING EQUATIONS AS PER IEEE 738 AND CIGRE 601

Standard	Equation	
IEEE 738	$q_j = I^2 \cdot R_{AC}(T_c)$	(7)
CIGRE TB 601	$P_J = k_{sk} \cdot I^2 \cdot R_{AC}(T_c)$	(8)

In (7) and (8), I is the RMS value of the current, and k_{sk} is the skin effect factor, respectively. For standard applications of conductor diameter and load frequency, the skin effect factor is below 2% [8]. The electrical resistance of the conductor, $R_{AC}(T_c)$, as represented in (9), is a function of temperature T.

$$R_{AC}(T_c) = \underbrace{\left[\frac{R(T_{high}) - R(T_{low})}{T_{high} - T_{low}}\right](T_c - T_{low}) + R(T_{low})}_{Linear\ Interpolation} \quad (1)$$

The values $R(T_{high})$ and $R(T_{low})$ represent the conductor resistance at high and low temperatures, respectively. These values are typically provided by the conductor manufacturer or can be obtained from standard handbooks for ACSR conductors. They are widely accepted within the professional community, as they incorporate magnetic effects, skin effect, and lay ratios. Using these reference points, the conductor resistance at any temperature T between T_{low} and T_{high} can be calculated through linear interpolation [10].

Solar heating refers to the heat generated by sunlight shining on the conductor. As shown in Table IV, the transfer of heat energy from solar radiation depends on several parameters, such as the sun's position, the intensity of solar radiation, the conductor's absorptivity, and its surface area [6]. The expressions used to model solar heating are defined differently in the IEEE 738 and CIGRÉ approaches, as detailed in Table IV [8].

In these equations, α and α_s represent the coefficients of solar radiation absorption, D denotes the conductor diameter, Q_s and I_T correspond to the global solar radiation intensities, and θ indicates the angle of solar incidence. While Q_s typically considers the direct solar component, I_T includes both incident and reflected solar radiation.

TABLE IV. SOLAR HEAT GAIN EQUATIONS AS PER IEEE 738 AND CIGRE 601

Standard	Equation	
IEEE 738	$q_s = \alpha \cdot D \cdot Q_{se} \cdot sin(\theta)$	(10)
CIGRE TB 601	$P_s = \alpha_s \cdot D \cdot I_T$	(11)

B. Convection and Radiative Cooling

Both IEEE and CIGRÉ standards calculate natural and forced convective cooling separately, as presented in Table V. Natural convective cooling takes place through the buoyant movement of heated air around the conductor in the absence of wind. This mechanism is described by (12) in the IEEE model and by (15) in the CIGRÉ model, respectively.

In contrast, forced convection is governed by wind, where the motion of air increases heat dissipation from the conductor, thereby enhancing the cooling effect. According to the IEEE standard, forced convection is represented by two different equations depending on wind speed: one applicable to low wind conditions and another to high wind speeds. In the CIGRÉ model, separate equations are also employed for natural convection in (15) and forced convection in (16). The heat loss rates due to both natural and forced convection are formulated in relation to the Nusselt number (N_u).

The thermal conductivity of the air layer in contact with the conductor is denoted as λ_f. The symbol T_s represents the surface temperature of the conductor, while T_a denotes the ambient air temperature. The Reynolds number (N_{Re}) characterizes the flow regime of air around the conductor. Lastly, K_{angle} refers to the angle of incidence coefficient, which accounts for the interaction angle between the airflow and the conductor surface.

The thermal conductivity of the air layer in contact with the conductor is denoted as λ_f. The symbol T_s represents the surface temperature of the conductor, while T_a denotes the ambient air temperature. The Reynolds number (N_{Re}) characterizes the flow regime of air around the conductor. Lastly, K_{angle} refers to the angle of incidence coefficient, which accounts for the interaction angle between the airflow and the conductor surface.

TABLE V. CONVECTIVE COOLING EQUATIONS AS PER IEEE 738 AND CIGRE 601

Standard	Cooling Type	Wind Speed, *Vw*	Equation	
IEEE 738	Natural	Zero	$q_c = 3.645 \cdot \gamma^{0.5} \cdot D^{0.75} \cdot (T_s - T_a)^{1.25}$	(12)
	Forced	Low	$q_{c1} = K_{angle} \cdot \left[1.01 + 1.35 \cdot N_{Re}^{0.52}\right] \cdot \lambda_f \cdot (T_s - T_a)$	(13)
	Forced	High	$q_{c2} = K_{angle} \cdot 0.754 \cdot N_{Re}^{0.6} \cdot \lambda_f \cdot (T_s - T_a)$	(14)
CIGRE TB 601	Natural	Zero	$P_{cn} = \pi \cdot \lambda_f \cdot (T_s - T_a) \cdot Nu\beta$	(15)
	Forced	High	$P_{cf} = \pi \cdot \lambda_f \cdot (T_s - T_a) \cdot Nu\delta$	(16)

For radiative cooling, the formulations provided by IEEE in (17) and CIGRÉ in (18) are nearly identical. As radiation typically constitutes a minor component of the total heat loss—especially under conditions where forced convection is present—the CIGRÉ method suggests computing radiative losses using the equation summarized in Table V.

$$q_r = D \cdot 17.8 \cdot \varepsilon \cdot \left[\frac{T_s + 273}{100}\right]^4 - \left[\frac{T_a + 273}{100}\right]^4 \quad (2)$$

$$P_r = \pi \cdot D \cdot \sigma_B \cdot \varepsilon \cdot \left(T_s + 273\right)^4 - \left(T_a + 273\right)^4 \quad (3)$$

The emissivity (ε) of a conductor is influenced by its surface condition, with values ranging from 0.27 for new stranded conductors to 0.95 for industrially weathered ones. A typical recommended value is 0.5. The Stefan–Boltzmann constant ($\sigma = 5.67 \times 10^{-8}$ W/m^{2}K^4) is used in the calculation of radiative heat loss. Ambient temperature is represented by T_a, and T_s denotes the conductor's surface temperature. These parameters are essential for determining heat loss due to radiation. The IEEE standard incorporates an empirical factor of 17.8, whereas the CIGRÉ method applies the Stefan–Boltzmann law for a more physically accurate calculation of radiative heat loss.

C. Comparison of IEEE 738 and CIGRÉ TB601: Solar Gain and Convective Cooling

The IEEE Std 738 and CIGRÉ TB 601 standards both provide methodologies for DLR of overhead TLs, but they differ in their treatment of environmental influences and conductor thermal behavior. IEEE Std 738 generally adopts a segmented and simplified approach, using average or worst-case environmental conditions and discretized conductor segments to estimate convective cooling and solar heat gain. In contrast, CIGRÉ TB 601 employs a more detailed and continuous representation, accounting for circumferential and angular variations in solar radiation and wind convection along the conductor surface. These methodological differences lead to variations in the calculated ampacity, especially under extreme or non-uniform environmental conditions. While IEEE Std 738 offers a standardized, conservative estimation suitable for regulatory purposes, CIGRÉ TB 601 provides a refined assessment that can better capture real-time conductor behavior, enabling more accurate utilization of transmission capacity. The differences in solar heat gain and convective cooling between the two standards are summarized in Tables VI and VII, respectively, which highlight the key assumptions and calculation approaches adopted in each methodology [8,10].

Table VI provides a detailed comparison of how IEEE Std 738 and CIGRÉ TB 601 handle solar heat gain. IEEE Std 738 uses average or worst-case irradiance values and does not fully account for conductor orientation or time-dependent variations, resulting in a conservative estimate of solar heating. In contrast, CIGRÉ TB 601 models solar radiation across the conductor circumference, including angular effects and diurnal changes, which enables a more realistic prediction of conductor temperatures. This refined modeling approach is particularly important for accurately determining ampacity during periods of high solar exposure, as it can identify available thermal headroom that would otherwise be overlooked using a simplified standard. Therefore, CIGRÉ's methodology allows transmission

TABLE VI. SOLAR HEAT GAIN COMPARISON AS PER IEEE 738 AND CIGRE 601

Feature/Parameter	IEEE Std 738	CIGRÉ TB 601	Notes/Impact
Solar irradiance assumption	Average or seasonal worst-case values	Circumferential and angular variation	CIGRÉ considers the exact position of the sun and conductor orientation, providing a more detailed heating profile, especially during peak solar hours.
Conductor orientation consideration	Limited	Explicitly considered	CIGRÉ evaluates heating differences across strands due to orientation, which can affect local conductor temperature.
Daily/seasonal variation	Simplified/constant	Continuous/ time-dependent	CIGRÉ captures diurnal and seasonal variations, allowing more accurate estimation of maximum temperatures throughout the day and year.
Effect on ampacity estimation	Conservative, lower estimate	More accurate, potentially higher	IEEE's simplified assumptions may underestimate available capacity, whereas CIGRÉ's approach supports better utilization of conductor thermal limits.

TABLE VII. CONVECTIVE COOLING COMPARISON AS PER IEEE 738 AND CIGRE 601

Feature/Parameter	IEEE Std 738	CIGRÉ TB 601	Notes/Impact
Convective model	Segmented, discrete coefficients	Continuous correlation	IEEE uses discrete segments that may over- or underestimate cooling in localized areas; CIGRÉ models smooth variations across the conductor circumference.
Wind direction/ incidence	Simplified or assumed	Explicitly modeled	CIGRÉ includes wind angle and incidence effects, providing more accurate convective heat removal calculations.
Conductor configuration consideration	Limited (single or bundled)	Detailed for bundled conductors	CIGRÉ accounts for sub-conductor interactions and spacing, which significantly affect airflow and convective efficiency.
Effect on ampacity estimation	Conservative, may under- or over-estimate locally	More accurate, smooth variations	Continuous modeling in CIGRÉ leads to more precise ampacity estimates, allowing better real-time utilization under variable wind conditions.

operators to exploit additional capacity safely, improving real-time line utilization.

Table VII presents a comparison of convective cooling treatments in IEEE Std 738 and CIGRÉ TB 601. IEEE Std 738 employs a segmented approach with discrete coefficients for each conductor segment, which can result in abrupt variations in predicted cooling and potentially conservative ampacity estimates. Conversely, CIGRÉ TB 601 applies a continuous correlation for convective heat transfer along the conductor circumference, explicitly considering wind direction, wind incidence, and the effects of bundled conductor configurations. This allows for a more realistic assessment of cooling efficiency under varying environmental conditions. By capturing subtle spatial variations in convection, CIGRÉ provides smoother and more accurate ampacity predictions, which is particularly relevant for real-time monitoring and dynamic utilization of TLs. The detailed treatment of convection also supports improved operational decision-making and reduces unnecessary conservative limitations on conductor loading [8,10].

D. Environmental Factors and System Description

This study investigates the available ampacity of a Hawk-type ACSR conductor installed on a 154 kV TL. The line is a three-phase, 50 Hz single-circuit system; it is aligned at an angle of 90° to the North. Details regarding the conductor configuration and technical specifications are provided in Fig. 2 and Table VIII. This study assesses the maximum ampacity of a TL using DLR, referencing both IEEE and CIGRÉ standards to ensure accurate calculation methods. The ampacity is determined using (2) for the IEEE approach and (4) for the CIGRÉ approach, considering varying weather conditions such as ambient temperature, wind speed, wind angle, and solar radiation.

1) Meteorological Data:

Spatial and temporal variations in local weather conditions, such as wind speed and direction, ambient air temperature, and solar radiation, significantly affect the capacity of TLs. Accurate data collection is essential for assessing DLR and understanding how weather factors influence TL performance. As presented in Table IX, meteorological data were collected from multiple sites to ensure comprehensive coverage and capture the variability along different TL sections.

To accurately assess the additional capacity of TLs and conduct a robust, representative analysis, weather data from six carefully selected sites were used. These sites were chosen for their ability to reflect localized environmental conditions, particularly air temperature variations and wind behavior, which are critical parameters in determining TL ampacity. For this study, data were sourced from Meteostat, with a focus on locations and days characterized by low wind speeds and elevated temperatures, representing the most thermally stressful conditions for the conductors. This approach ensures that the modeling framework developed is both conservative and realistic, enhancing the reliability of real-time TL performance assessments under varying atmospheric conditions. The weather data collected for this study focus on two distinct scenarios: the hottest day of summer and a typical day in winter. By analyzing these contrasting conditions, the study offers a thorough understanding of how weather variations influence TL performance.

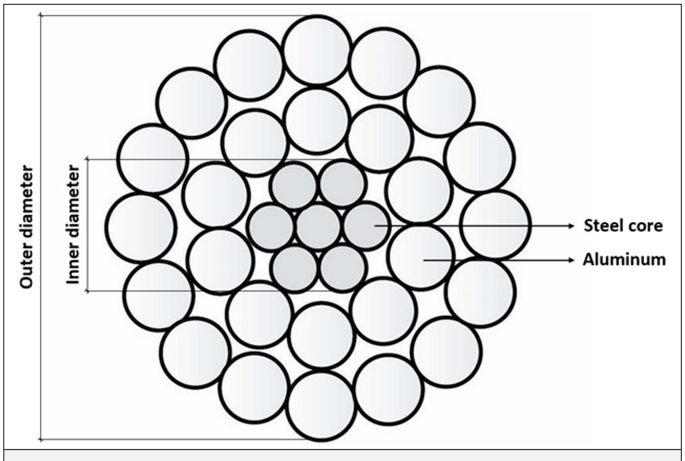

Fig. 2. Configuration of Hawk-type ACSR conductor.

TABLE VIII. HAWK ACSR CONDUCTOR SPECIFICATIONS

Parameter	Value	Parameter	Value
Rated section (MCM)	477	Number of layers	3
Total conductor area (mm^2)	281.14	Aluminum wires (Number)	26
Aluminum area (mm^2)	241.7	Aluminum wire diameter (mm)	3.44
Diameter (mm)	21.8	Steel wires (Number)	7
Heat elongation coefficient (1/°C)	0.0000189	Steel wire diameter (mm)	2.67
DC resistance (ohm/km @ 20°C)	0.1169	Summer capacity (MVA)	110
AC resistance (ohm/km @ 25°C)	0.1198	Spring/winter capacity (MVA)	180
AC resistance (ohm/km @ 75°C)	0.1432	Maximum conductor temperature (°C)	75

2) Summer Day Conditions:

The hottest summer day, illustrated in Figs. 3, 4, and 5—depicting wind speed, ambient temperature, wind angle, and solar gain, respectively—presents extreme environmental conditions that place significant thermal stress on TL operation. On this day, the combined effect of high ambient temperatures, low wind speeds, and intense solar radiation creates a challenging scenario, severely limiting the conductor's ability to dissipate heat effectively.

TABLE IX. METEOROLOGICAL DATA WEBSITES

No	Weather Provider	Website Link
1	Weather Underground	https://www.wunderground.com
2	Meteostat	https://meteostat.net
3	Time and Date	https://www.timeanddate.com/weather
4	AccuWeather	https://www.accuweather.com
5	Dark Sky	https://darksky.net
6	NOAA Climate Data Online (CDO)	https://www.ncdc.noaa.gov/cdo-web

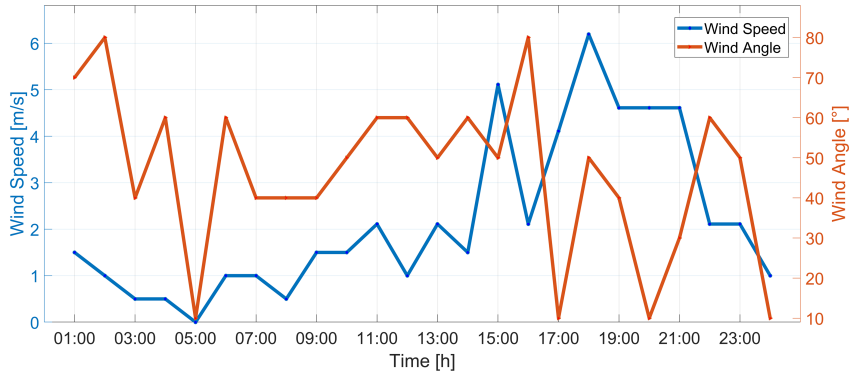

Fig. 3. Wind speed and wind angle variation over a 24-hour summer period.

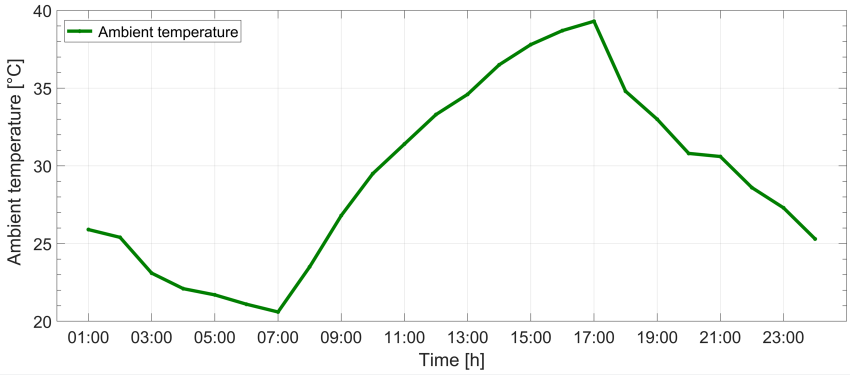

Fig. 4. Ambient temperature variation over a 24-hour summer period

Wind speed exhibits significant fluctuations throughout the day, typically remaining low during midday when ambient temperatures peak. This reduction in wind speed limits convective cooling, resulting in elevated conductor temperatures. As illustrated in Fig. 3, both wind speed and wind angle vary considerably. Wind speeds range from 0 m/s to over 6 m/s, with an average summer speed of 2.17 m/s, indicating that seasonal wind conditions are often inconsistent and may not provide adequate cooling for overhead conductors. Wind angle also plays a critical role in determining line ampacity. Convective cooling is most effective when the wind angle approaches 90°, whereas angles closer to 0° are less efficient, even in the presence of wind. Wind angles range from a minimum of 10° to a maximum of 80°, with an average value greater than 45°, which is generally considered favorable for enhancing convective heat dissipation.

Ambient temperature follows a clear diurnal pattern, peaking during midday and declining at night. The high daytime temperatures contribute to elevated conductor temperatures. In Fig. 4, the lowest temperature is 20.6°C, and the highest is 39.3°C, with an average of 24°C. These values reflect a characteristically hot seasonal climate, which poses thermal stress on TL operation.

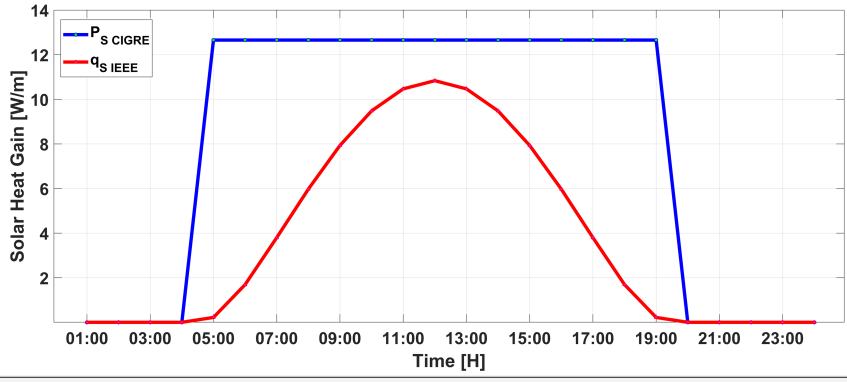

Fig. 5. Solar heat gain profile according to IEEE and CIGRE in summer.

As illustrated in Fig. 5, both IEEE and CIGRÉ standards offer methodologies for calculating solar gain, with the IEEE approach utilizing (10) and the CIGRÉ model employing (11). On the hottest summer days, solar radiation reaches peak intensity around midday due to the high solar elevation angle. This elevated solar input significantly increases the heat absorbed by the conductor, leading to a notable rise in its surface temperature. The resulting solar gain presents a considerable challenge to maintaining thermal equilibrium, as the conductor relies primarily on convective and radiative cooling to dissipate the excess heat. The combination of intense solar radiation and elevated ambient temperatures reduces the overall cooling efficiency, underscoring the importance of accurate thermal modeling to prevent overheating and ensure the safe operation of the TL.

3) Winter Day Conditions:

The typical winter day is illustrated in Figs. 6, 7, and 8, which present data on wind speed, ambient temperature, wind angle, and solar gain. On this day, the combination of lower ambient temperatures, higher wind speeds, and reduced solar radiation creates favorable conditions for heat dissipation. These factors collectively enhance the cooling performance of the conductor, allowing it to maintain lower operating temperatures compared to hot summer conditions.

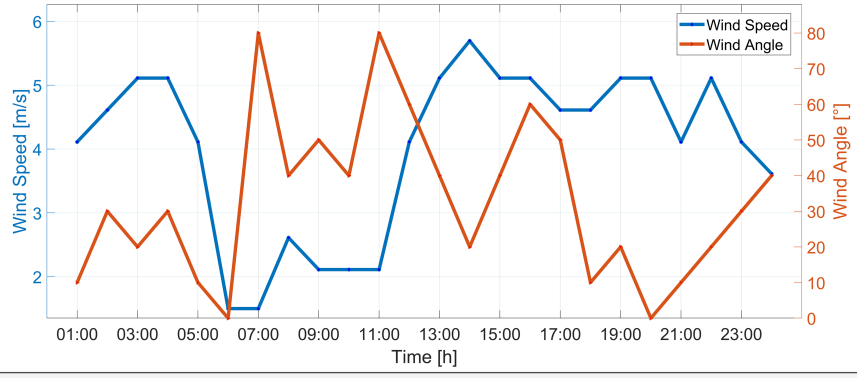

Fig. 6. Wind speed and wind angle variation over a 24-hour winter period.

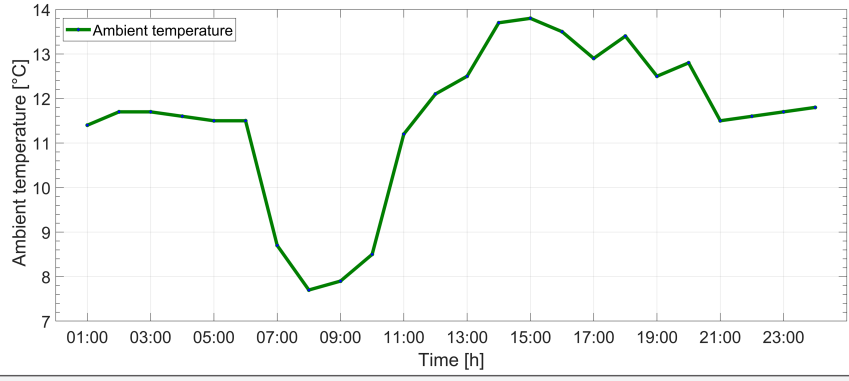

Fig. 7. Ambient temperature variation over a 24-hour winter period.

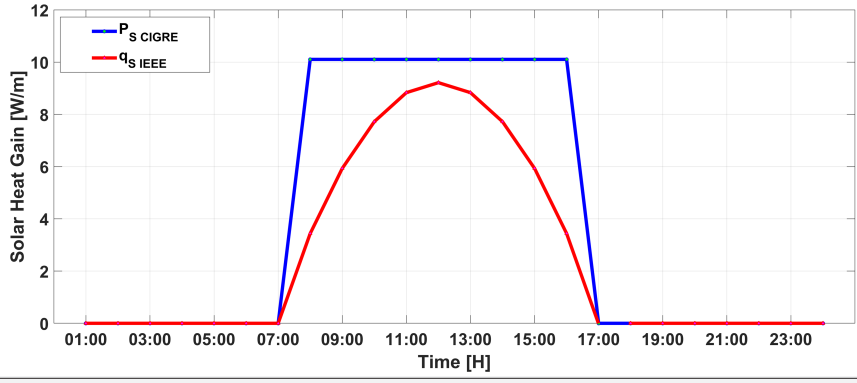

Fig. 8. Solar heat gain profile according to IEEE and CIGRE in winter.

Wind speed is relatively higher in winter compared to the hottest summer days, enhancing convective cooling throughout the day. Additionally, wind speed variations are less pronounced, providing more consistent cooling conditions. As shown in Fig. 6, both wind speed and wind angle exhibit noticeable variation, with wind speeds ranging from 1.5 m/s to over 5.6 m/s and an average winter wind speed of 4.01 m/s—conditions generally favorable for effective conductor cooling. Wind angle also plays a significant role in determining line ampacity. Convective cooling is most effective when the wind angle approaches 90°, while angles near 0° reduce the cooling effect despite the presence of wind. In Fig. 6, wind angles range from 0° to a maximum of 80°, with an average of less than 45°, an orientation typically considered less favorable for optimal convective heat dissipation.

Ambient temperature remains low throughout the day, with minimal fluctuations. The reduced temperature gradient between the conductor and the surrounding air enhances the efficiency of convective heat transfer. As shown in Fig. 7, the minimum temperature is 7.7°C, and the maximum is 13.8°C, with an average of 11.55°C. These values indicate that the seasonal weather conditions are relatively cold, favoring improved thermal management of the conductor.

In Fig. 8, both IEEE and CIGRÉ standards provide methods for calculating solar gain, with IEEE utilizing (10) and CIGRÉ applying (11). On a typical winter day, solar radiation is considerably lower due to the sun's reduced altitude in the sky. This diminished solar intensity results in less heat being absorbed by the conductor, thereby contributing minimally to conductor heating. The reduced solar gain, coupled with the generally lower ambient temperatures, significantly improves the overall cooling efficiency of the TL, enabling it to operate at higher ampacity while experiencing less thermal stress.

Comparing these two scenarios effectively demonstrates how environmental factors such as wind speed, wind angle, ambient temperature, and solar radiation influence the ampacity of TLs. Incorporating this comprehensive weather data into calculations allows for more accurate predictions of available ampacity under diverse conditions, thereby enhancing the efficiency and reliability of the power transmission system.

III. RESULTS AND DISCUSSION

The analysis was performed using data collected from various sites, as outlined in Table IX, with a 1-hour resolution. The data covers one extremely hot summer day (June 25, 2024) and one typical winter day (January 20, 2024). This timeframe was chosen to ensure both summer and winter conditions are accounted for, providing a more comprehensive and reliable assessment of the line's capacity. By evaluating the TL's performance under extreme heat and moderate cold, factors such as wind speed, ambient temperature, solar radiation, and wind angle were considered. This approach offers valuable insights into how the TL behaves under varying seasonal and environmental conditions, ultimately improving the understanding of its dynamic capacity.

This section first analyzes the conductor's temperature under real load conditions, as illustrated in Figs. 3, 4, and 5 for summer and Figs. 6, 7, and 8 for winter, using (5) and (6) for IEEE and CIGRÉ, while considering all relevant weather conditions at that time. The analysis shows the conductor's surface temperature under varying conditions, providing a comprehensive understanding of how different environmental factors influence its thermal behavior.

. One hour after current begins flowing through the conductor, the surface temperature rises to 28.35°C. This increase is primarily influenced by Joule heating (5.36 W/m), zero solar heat gain, radiative cooling (0.035 W/m), and convective cooling (0.79 W/m). The values of P_c and P_r are calculated based on wind speed, wind direction, and ambient temperature, as shown in Figs. 3, 4, and 5.

However, between 03:00 and 04:00, the conductor temperature decreases despite an increase in load current from 200.9 A to 214.2 A. During this period, the wind speed remains steady at 0.5 m/s, the wind direction shifts from 40° to 60°, the ambient temperature drops from 23.1°C to 21.1°C, and solar heat gain is zero. According to the IEEE standard, Joule heating is calculated as 5.55 W/m, radiative cooling as 1.381 W/m, and convective cooling as 5.694 W/m, resulting in a surface temperature decrease from 27.89°C to 27.19°C. Similarly, under the CIGRÉ standard, Joule heating is calculated as 5.54 W/m, radiative cooling as 1.74 W/m, and convective cooling as 5.62 W/m, leading to a surface temperature drop from 27.58°C to 26.75°C. Despite the increase in current, which would typically lead to higher Joule heating, the cooling effect due to the change in wind angle was more significant. Additionally, the drop in ambient temperature further enhanced the cooling effect, causing a reduction in the conductor surface temperature even with the increase in current.

However, between 10:00 and 11:00, the conductor surface temperature increases despite a decrease in load current from 150.1 A to 141.6 A. During this period, the wind speed rises from 1.5 m/s to 2.1 m/s, the wind direction shifts from 40° to 50°, and the ambient temperature increases from 26.8°C to 29.5°C. Additionally, solar heat gain increases from 7.9 W/m to 9.4 W/m according to the IEEE standard, and up to 12.65 W/m according to the CIGRÉ standard, as shown in Figs. 3, 4, and 5. Based on the IEEE standard, Joule heating is calculated as 2.49 W/m, radiative cooling as 1.06 W/m, and convective cooling as 8.75 W/m, resulting in a surface temperature rise from 35.49°C to 36.95°C. Under the CIGRÉ standard, Joule heating is 2.5 W/m, radiative cooling is 2.02 W/m, and convective cooling is 11.838 W/m, leading to a temperature increase from 37.21°C to 37.8°C. Between 05:00 and 19:00, the conductor temperature calculated using the CIGRÉ standard is consistently higher than that of the IEEE standard due to the higher solar heat gain, which remains constant at 12.65 W/m. This temperature rise can be attributed to the combined effect of the increased solar radiation and the higher ambient temperature, which, despite the reduction in current, led to a net increase in the heat absorbed by the conductor, overriding the effect of the reduced load current.

As shown in Fig. 10, the conductor surface temperature reflects the thermal behavior of the line during a typical winter day, illustrating how environmental factors such as ambient temperature, wind speed, and solar radiation influence the conductor's thermal dynamics.

In Fig. 10, the surface temperature is assumed to be 12°C at 01:00, equal to the ambient temperature. After 1 hour of carrying a current of 356 A, the conductor's surface temperature rises to 18°C, indicating that the surface temperature lags slightly behind the current flowing through the conductor. From 01:00 to 02:00, the current through the conductor decreases from 365 A to 342.6 A. As shown in the figure, the surface temperature also decreases under both standards, but

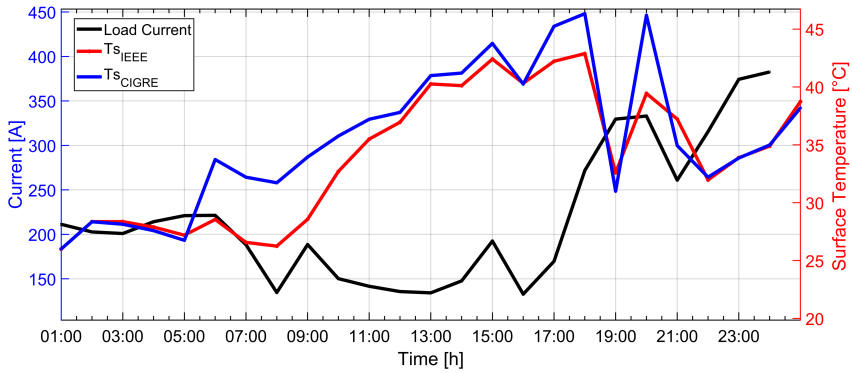

Fig. 9. Variation of load current and conductor surface temperature based on IEEE and CIGRÉ standards in summer.

with different values. According to the IEEE standard, Joule heating is calculated as 13.65 W/m, radiative cooling as 1.35 W/m, and convective cooling as 17.65 W/m, resulting in a surface temperature drop from 18°C to 15.55°C. Similarly, under the CIGRÉ standard, Joule heating is 13.64 W/m, radiative cooling is 1.78 W/m, and convective cooling is 19.28 W/m, leading to a temperature decrease from 18°C to 14.52°C. These values for Joule heating, radiative cooling, and convective cooling are derived from Figs. 6, 7, and 8, respectively.

As shown in Fig. 10, at certain times, the difference between the two standards becomes more noticeable. For instance, between 08:00 and 09:00, the surface temperature difference between the IEEE and CIGRÉ standards reaches approximately 3°C. According to the IEEE standard, Joule heating is calculated at 7.05 W/m, radiative cooling at 1.65 W/m, convective cooling at 17.56 W/m, and solar heat gain increases from 3.4 to 5.9 W/m. In contrast, under the CIGRÉ standard, Joule heating is 7.04 W/m, radiative cooling is 2.089 W/m, convective cooling is 16.571 W/m, and solar heat gain remains constant at 10.1 W/m throughout the day. Although all parameters influence temperature variation, at this time, solar heat gain appears to have the most significant impact. This is evident in the consistently higher surface temperature observed under the CIGRÉ standard. These values for Joule heating, radiative cooling, and convective cooling are derived from Figs. 6, 7, and 8, respectively.

Taking into account the environmental conditions for both summer and winter, and applying the internationally recognized IEEE and CIGRÉ standards, the conductor's ampacity under steady-state conditions has been accurately calculated using (2) and (4) at its maximum surface temperature. This calculation evaluates DLR and assesses TL's optimal performance under varying environmental conditions. As shown in Figs. 11 and 12 for summer and winter, respectively, the analysis demonstrates how seasonal variations significantly affect the ampacity and efficiency of the TL.

According to Table VIII, the static line rating (SLR) of the overhead TL was set at 412.4 A for the summer season, corresponding to its designed ampacity. As shown in Fig. 11, the ampacity calculated using DLR reveals noticeable differences between the two standards at certain points. Specifically, at 01:00, the ampacity calculated using the CIGRÉ standard is higher than that of the IEEE standard. The primary factor contributing to this difference is convective cooling, with CIGRÉ estimating it at 88.212 W/m, while IEEE calculates it at 86.2 W/m. These values were derived from Figs. 3, 4, and 5, with a wind speed of 1.5 m/s, an ambient temperature of 25.9°C, and a wind angle of 70°. In low wind speed conditions, the CIGRÉ method places greater emphasis on the impact of wind angle, resulting in a higher ampacity calculation compared to the IEEE method. These findings underscore the importance of considering environmental factors and the assumptions inherent to each standard in accurately determining the ampacity of overhead TLs.

Additionally, at 05:00, a significant difference is observed between the two standards, with the ampacity calculated using the CIGRÉ method being lower than that of the IEEE method. This discrepancy primarily arises from the difference in solar heat gain, which is estimated by CIGRÉ at 12.65 W/m, whereas IEEE calculates it as 0.218 W/m. The convective cooling values show only a slight difference,

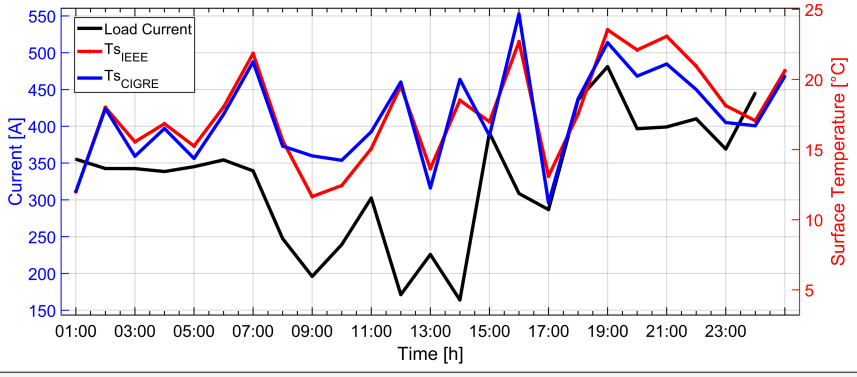

Fig. 10. Variation of load current and conductor surface temperature based on IEEE and CIGRÉ standards in winter.

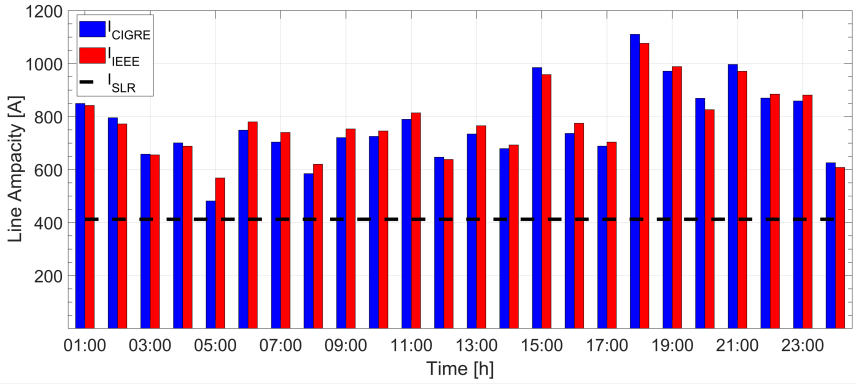

Fig. 11. Line ampacity variation in summer based on IEEE and CIGRÉ standards with SLR reference.

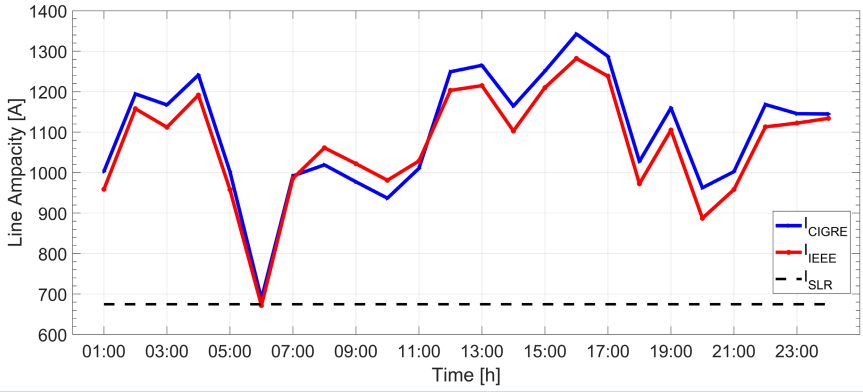

Fig. 12. Line ampacity variation in winter based on IEEE and CIGRÉ standards with SLR reference.

with CIGRÉ at 29.8 W/m and IEEE at 30.43 W/m. These values were derived from Figs. 3, 4, and 5, with a wind speed of 0 m/s, an ambient temperature of 21.7°C, and a wind angle of 10°. A key distinction between the two methods lies in their treatment of solar heat gain: the CIGRÉ method assumes it to be constant, while the IEEE method accounts for its variation throughout the day. As a result, the ampacity calculated by CIGRÉ is lower than that calculated by IEEE during this time. This comparison emphasizes the importance of considering varying environmental factors and their treatment in each standard, ultimately influencing the calculated ampacity and performance of the TL.

However, at 18:00, the ampacity calculated by CIGRÉ exceeds that of IEEE. The primary differences between the two methods are found in both solar heat gain and convective cooling. Specifically, CIGRÉ estimates the solar heat gain at 12.65 W/m, while IEEE calculates it as 1.69 W/m. Additionally, the convective cooling values are higher in CIGRÉ, with 176.38 W/m compared to 154.74 W/m in IEEE. These values were derived from Figs. 3, 4, and 5, using a wind speed of 6.1 m/s, an ambient temperature of 34.8°C, and a wind angle of 50°. A key distinction between the two methods is that in the CIGRÉ method, high wind speed has a more pronounced effect on convective cooling, while in IEEE, the effect is less significant. Furthermore, solar heat gain is considered constant in CIGRÉ, whereas it varies throughout the day in IEEE. As a result, the ampacity calculated by CIGRÉ is higher than that of IEEE during this period. This comparison underscores the significant influence of wind speed and solar heat gain assumptions on the calculated ampacity, illustrating how different environmental factors are handled in each standard.

According to Table VIII, the overhead TL is rated for a SLR of 674.8 A during the winter season, reflecting its designed current-carrying capacity. Fig. 12 illustrates notable differences in ampacity values calculated using the IEEE and CIGRÉ standards. At 06:00, the ampacity based on the IEEE method is lower than those of the CIGRÉ method and the SLR. This difference primarily arises from convective cooling, estimated as 49.5 W/m by CIGRÉ and 46.3 W/m by IEEE. These values were calculated using Figs. 6, 7, and 8, considering a wind speed of 1.5 m/s, an ambient temperature of 11.5°C, and a wind angle of 0°. Under adverse weather conditions, such as low wind speed and high ambient temperature, DLR may require a lower current limit than the SLR. This reduction is necessary to prevent conductor overheating and excessive sag, ensuring safe operation within thermal limits. Limiting the current helps protect the TL from potential damage due to thermal stress, thereby reducing the risk of failure [11, 36]. Between 07:00 and 11:00, the IEEE ampacity exceeds that of CIGRÉ. This trend aligns with the wind and temperature profiles presented in Figs. 6 and 7, where wind speeds remain below 2.5 m/s and ambient temperatures are relatively low. For the remainder of the day, however, the CIGRÉ ampacity is generally higher than the IEEE value. This outcome is attributed to increased wind speeds during winter, with an average value of 4.17 m/s as indicated in Fig. 6. Under higher wind conditions, the CIGRÉ method tends to estimate greater convective cooling, leading to higher ampacity values compared to IEEE. These findings highlight the influence of wind speed

on ampacity calculations and the impact of methodological differences between the IEEE and CIGRÉ approaches in varying environmental conditions.

IV. CONCLUSION

This study highlights the important role of DLR in improving power transmission systems by allowing real-time adjustments based on environmental conditions. Unlike traditional SLR, which relies on fixed, conservative assumptions and often results in underused transmission capacity, DLR uses real-time weather and load data to continuously update ampacity values. By comparing the IEEE Std 738 and CIGRÉ TB 601 standards, both based on the heat balance principle but differing in their methods and sensitivity to parameters, this paper shows how ampacity changes under different environmental conditions.

The results demonstrate that DLR provides a significant improvement over static ratings, with both the IEEE and CIGRÉ methods increasing average ampacity by over 35% in both summer and winter. Seasonal variations show that ampacity is much higher in winter—26.9% higher for IEEE and 29.8% higher for CIGRÉ—due to cooler temperatures and higher wind speeds, which enhance convective cooling. Additionally, the study finds that the CIGRÉ method predicts higher ampacity under high wind conditions, while the IEEE method works slightly better in low wind situations.

These findings emphasize the need to select the right standard based on local climate conditions and the requirements of the power network. Using DLR effectively could reduce the need for expensive infrastructure upgrades, improve the integration of renewable energy, and make the grid more flexible, efficient, and resilient.

Future research could look into challenges in implementing DLR in real-time, its integration with grid management systems, and how sensor accuracy and data delays affect its performance. Expanding the study to consider DLR behavior during faults or emergencies could provide more insights into its reliability in real-world situations.

Data Availability Statement: The data that support the findings of this study are available on request from the corresponding author.

Peer-review: Externally peer-reviewed.

Author Contributions: Concept – CF.K., Z.Z.; Design – Z.Z.; Supervision – CF.K.; Resources – CF.K.; Materials – CF.K., Z.Z.; Data Collection and/or Processing – CF.K., Z.Z.; Analysis and/or Interpretation – CF.K., Z.Z.; Literature Search – CF.K., Z.Z.; Writing – CF.K., Z.Z.; Critical Review – CF.K.

Declaration of Interests: The authors have no conflicts of interest to declare.

Funding: The research work was conducted with the financial supports of Scientific and Technological Research Council of Türkiye (TÜBİTAK) under the 1002 program, grant number 125E406.

REFERENCES

1. U.S. Dept. of Energy, *"Dynamic line rating systems for transmission lines: American Recovery and Reinvestment Act of 2009," Washington, DC, USA*, Tech. Rep., 2014.
2. G. I. Rashed, D. Otuo-Acheampong, A. A. Mensah, and H. Haider, "Comparison of metaheuristic optimization techniques for the optimal placement and sizing of shunt flexible alternating current transmission systems device considering load increase," *Electrica*, vol. 23, no. 3, 2023.
3. X. Zhang, C. Jiang, H. Huang, F. Zhang, W. Luo, and N. Rana, "Automatic classification of transmission lines based on edge detection filtering algorithm and laser point cloud data processing," *Electrica*, vol. 23, no. 2, pp. 231–239, 2023. [CrossRef]
4. U.S. Dept. of Energy, *"Smart grid system report," Washington, DC, USA*, Tech. Rep., 2010.
5. Z. Zia, and C. F. Kumru, *Comparative Analysis of IEEE and CIGRE Standards for Dynamic Line Rating: Impact of Environmental Factors on Ampacity Calculations*, 2025.
6. B. P. Bhattarai et al., "Transmission line ampacity improvements of altalink wind plant overhead tie-lines using weather-based dynamic line rating," in *IEEE Power Energy Soc. Gen. Meet.*, vol. 2017: IEEE, pp. 1–5, 2017.
7. Y. Su, J. Teh, Q. Luo, K. Tan, and J. Yong, "A two-layer framework for mitigating the congestion of urban power grids based on flexible topology with dynamic thermal rating," *Prot. Control Mod. Power Syst.*, vol. 9, no. 4, pp. 83–95, 2024. [CrossRef]
8. J. Iglesias et al., *Guide for Thermal Rating Calculations of Overhead Lines*. Paris, France: CIGRE, 2014.
9. A. W. Abboud, J. P. Gentle, K. Parikh, and J. Coffey, *Sensitivity Effects of High Temperature Overhead Conductors to Line Rating Variables*. Idaho National Laboratory (INL), Idaho Falls, ID (United States), 2020.
10. "Transmission and D. Committee," *IEEE Std*, vol. 2012, 738TM, *2012: IEEE standard for calculating the current-temperature relationship of bare overhead conductors ed: IEEE New York*.
11. B. P. Bhattarai et al., "Improvement of transmission line ampacity utilization by weather-based dynamic line rating," *IEEE Trans. Power Deliv.*, vol. 33, no. 4, pp. 1853–1863, 2018. [CrossRef]
12. X. He, and J. Teh, "Impacts of dynamic thermal rating systems on wind generations: A review," *Electr. Power Syst. Res.*, vol. 233, p. 110492, 2024. [CrossRef]
13. T. Song, J. Teh, and B. Alharbi, "Reliability impact of dynamic thermal line rating and electric vehicles on wind power integrated networks," *Energy*, vol. 313, p. 133945, 2024. [CrossRef]
14. J. Teh, and C.-M. Lai, "Reliability impacts of the dynamic thermal rating and battery energy storage systems on wind-integrated power networks," *Sustain. Energy Grids Netw.*, vol. 20, p. 100268, 2019. [CrossRef]
15. J. L. Aznarte, and N. Siebert, "Dynamic line rating using numerical weather predictions and machine learning: A case study," *IEEE Trans. Power Deliv.*, vol. 32, no. 1, pp. 335–343, 2017. [CrossRef]
16. Y. Cong, P. Regulski, P. Wall, M. Osborne, and V. Terzija, "On the use of dynamic thermal-line ratings for improving operational tripping schemes," *IEEE Trans. Power Deliv.*, vol. 31, no. 4, pp. 1891–1900, 2016. [CrossRef]
17. F. Qiu, and J. Wang, "Distributionally robust congestion management with dynamic line ratings," *IEEE Trans. Power Syst.*, vol. 30, no. 4, pp. 2198–2199, 2015. [CrossRef]
18. M. Nick, O. Alizadeh-Mousavi, R. Cherkaoui, and M. Paolone, "Security constrained unit commitment with dynamic thermal line rating," *IEEE Trans. Power Syst.*, vol. 31, no. 3, pp. 2014–2025, 2016. [CrossRef]
19. J. P. Gentle, K. S. Myers, J. W. Bush, S. A. Carnohan, and M. R. West, "Dynamic line rating systems: Research and policy evaluation," in IEEE PES General Meeting| Conference & Exposition, 2014, pp. 1–5. [CrossRef]
20. J. Teh, C.-M. Lai, and Y.-H. Cheng, "Impact of the real-time thermal loading on the bulk electric system reliability," *IEEE Trans. Reliab.*, vol. 66, no. 4, pp. 1110–1119, 2017. [CrossRef]
21. N. H. Abas, M. Z. A. Ab Kadir, N. Azis, J. Jasni, N. F. A. Aziz, and Z. M. Khurshid, "Optimizing grid with dynamic line rating of conductors: A comprehensive review," *IEEE Access*, vol. 12, pp. 9738–9756, 2024. [CrossRef]
22. M. Constantin et al., "Dynamic rating technology approach for real-time monitoring of overhead transmission lines," in International Conference and Exposition on Electrical And Power Engineering (EPE), 2022, pp. 7–12. [CrossRef]
23. L. Rácz, B. Németh, G. Göcsei, D. Zarchev, and V. Mladenov, "Performance analysis of a dynamic line rating system based on project experiences," *Energies*, vol. 15, no. 3, p. 1003, 2022. [CrossRef]
24. T. Konstantinou, N. Savvopoulos, and N. Hatziargyriou, "Probabilistic ampacity forecasting for overhead transmission lines," in International Conference on Smart Energy Systems and Technologies (SEST), 2019, pp. 1–6. [CrossRef]
25. E. Carlini, F. Massaro, and C. Quaciari, "Methodologies to uprate an overhead line. Italian TSO case study," *J. Electr. Syst.*, vol. 9, no. 4, 2013.
26. E. Ali, and A. M. Knight, "An enhanced algorithm for conventional protection devices of transmission lines with DTLR," *IEEE Access*, vol. 9, pp. 147295–147305, 2021. [CrossRef]

27. J. Johnson et al., *Dynamic Line Rating Oncor Electric Delivery Smart Grid Program*. Gaithersburg, United States of America: Oncor Electric Delivery Company Llc, 2013.
28. J. R. Young, *Smart Grid Technology in the Developing World*, 2017.
29. J. Teh, "Uncertainty analysis of transmission line end-of-life failure model for bulk electric system reliability studies," *IEEE Trans. Reliab.*, vol. 67, no. 3, pp. 1261–1268, 2018. [CrossRef]
30. O. A. Lawal, and J. Teh, "Assessment of dynamic line rating forecasting methods," *Electr. Power Syst. Res.*, vol. 214, p. 108807, 2023. [CrossRef]
31. O. A. Lawal, and J. Teh, "Dynamic line rating forecasting algorithm for a secure power system network," *Expert Syst. Appl.*, vol. 219, p. 119635, 2023. [CrossRef]
32. T. Song, and J. Teh, "Dynamic thermal line rating model of conductor based on prediction of meteorological parameters," *Electr. Power Syst. Res.*, vol. 224, p. 109726, 2023. [CrossRef]
33. O. A. Lawal, and J. Teh, "A framework for modelling the reliability of dynamic line rating operations in a cyber–physical power system network," *Sustain. Energy Grids Netw.*, vol. 35, p. 101140, 2023. [CrossRef]
34. O. A. Lawal, J. Teh, B. Alharbi, and C.-M. Lai, "Data-driven learning-based classification model for mitigating false data injection attacks on dynamic line rating systems," *Sustain. Energy Grids Netw.*, vol. 38, p. 101347, 2024. [CrossRef]
35. V. T. Morgan, "Rating of bare overhead conductors for continuous currents," in *Proc. Inst. Electr. Eng. UK*, vol. 114, no. 10: IET, pp. 1473–1482, 1967. [CrossRef]
36. L. Rácz, and B. Németh, "Dynamic line rating—An effective method to increase the safety of power lines," *Appl. Sci.*, vol. 11, no. 2, p. 492, 2021. [CrossRef]

Ziauddin Zia received his B.Sc. degree from Electrical Engineering from Alberoni University (Kapisa, Afghanistan) in 2018 and his M.Sc. degree in Electrical and Electronics Engineering from Suleyman Demirel University, Isparta, Türkiye, in 2025. His research interests include power system optimization and dynamic line rating.

Celal Fadil Kumru earned his Ph.D. in Electrical Engineering from Yıldız Technical University in 2016. He served as a research assistant between 2010 and 2020. Currently, he is an Assistant Professor at Suleyman Demirel University, Department of Electrical-Electronics Engineering. His main research areas are high voltage engineering, power system analysis, outdoor insulation, high voltage cables, and energy transmission and distribution systems.